Original Article

Reducing The Respiratory Motion Artifacts in PET Cardiology: A Simulation Study

Kourosh Ebrahim Nejad Gorji[1], Hossein Rajabi[1], Ebrahim Hajizadeh[2], Faraz Kalantari[1], Hadi Taleshi[1]

[1]Department of Medical Physics, [2]Department of Biostatistics, Tarbiat Modares University, Tehran, Iran

(Received 18 February 2007, Revised 12 March 2007, Accepted 25 March 2007)

ABSTRACT

Introduction: There are several technical features that make PET an ideal device for the noninvasive evaluation of cardiac physiology. Organ motion due to respiration is a major challenge in diagnostic imaging, especially in cardiac PET imaging. These motions reduce image quality by spreading the radiotracer activity over an increased volume, distorting apparent lesion size and shape and reducing both signal and signal-to-noise ratio levels

Methods: 4D average male torso (2 cm diaphragmatic motion) produced by NCAT phantom was used for simulations. Emission sinograms generated by Eidolon PET simulator were reconstructed using iterative algorithm using STIR. The respiratory motion correction (*RMC*) applied to data sets using an automatic algorithm. Cross section views, activity profiles, contrast-to-noise ratios and left ventricle myocardium widths of corrected and non-corrected images were compared to investigate the effect of applied correction.

Results: Comparison of respiratory motion corrected and non corrected images showed that the algorithm properly restores the left ventricle myocardium width, activity profile and improves contrast-to-noise ratios in all cases. Comparing the contrast recovery coefficient (Q_m)shows that the applied correction effected phases of number 7,8 and 9 of cardiac cycle more than the other 13 phases and the maximum value being 1.43±0.07 for phase number 8. The maximum value of ratio of the left ventricle myocardium width for non-*RMC* and *RMC* images along the line profile passing the apicobasal direction and along the line profile passing from the middle of the lateral wall of the left ventricle were 1.38±0.07 for phase number 9 and 1.12±0.03 for phases of number 8 and 9 respectively**.**

Conclusion: Blurring and ghosting of each image depends on the speed of diaphragm during that respiratory phase. This simulation study demonstrates that respiratory motion correction has good overall effect on PET cardiac images and can reduces errors originating from diaphragmatic motion and deformation. Effect of such a correction varies from one cardiac phase to another and this depends on the blurring and ghosting of all respiratory phases used to form this cardiac phase. Using an automatic algorithm capable of correcting respiratory motion using full signal may be very useful to prevent lengthening of the overall scan time to obtain same motionless lesion signal levels.

Key words: PET, Cardiology, Respiratory motion, Eidolon, Monte Carlo.

Iran J Nucl Med 2007; 15(2): 49-57

Corresponding Author: Dr. Hossein Rajabi, Department of Medical Physics, Tarbiat Modares University, Tehran, Iran, E-mail: hrajabi@modares.ac.ir

Introduction

By 2020 heart disease and stroke will become the leading cause of both death and disability worldwide, with the number of fatalities projected to increase to more than 20 million a year and to more than 24 million a year by 2030. Although there are several technical features that make Positron Emission Tomography (PET) an ideal device for the noninvasive evaluation of cardiac physiology (1), but organ motion due to respiration is a major challenge in diagnostic imaging, and especially in cardiac PET imaging that requires long scan times (typically 20-30 min for a whole-body scan) where data must be acquired over many respiratory cycles to obtain adequate statistics (2-4). During normal respiration with 2 cm diaphragmatic motion (5), cardiac images can be affected. Cardiac and respiratory motion during the data acquisition cause serious ghosting and blurring artifacts in imaging (6, 7) and these motions certainly have an impact on cardiac PET studies as well. Fitzpatrick et al showed that the variation in the magnitude of the errors in the cardiac uptake varied considerably with cardiac cycle less than with respiratory cycle (3). Respiratory motion reduces image quality by spreading the radiotracer activity over an increased volume (8), distorting apparent lesion and tumor location (9) and shape (10), and reducing both signal and signal-to-noise ratio (SNR) levels (11). Nehmeh et al demonstrate that any increase in the apparent lesion size will decrease the activity concentration per pixel within the lesion, resulting in a lesion contrast reduction (12). Different groups showed that respiratory motion artifacts in myocardium usually leads to a reduction in the myocardial activity estimation due to the heart and diaphragm motion during the data acquisition (13-15).

One solution is to use respiratory gating technique (16). Feasibility and usefulness of the technique has been shown on both phantom and patient studies (4, 17- 23). For gating, just a fraction of the PET scan is used during each respiratory cycle and this, as a major drawback, lengthens the overall scan time to obtain the same motionless lesion signal levels (4). This increase in the scan time may cause some difficulties caused by patient discomfort and immobilization (4, 24).

The purpose of this study was to investigate a new automatic algorithm for respiratory motion correction using the full signal across the entire respiratory cycle. Essentially, the respiratory cycle is divided into many short time steps which the signal data are acquired over these steps, and then grouped into several bins along the phase of respiration. Similar to works by Klein et al and Thorndyke et al, resulted bins are registered one-by-one and stacked on top of one another using an automatic algorithm to form a composite image related to a single point in the respiratory cycle. Using the entire respiratory cycle and not just the end of inspiration and expiration to perform the respiratory motion correction improves the signal and SNR level without increasing the scan time (4, 25-26).

In this study, first we proposed and investigated a new automatic algorithm and then we applied the algorithm to torso phantom data with respiratory and cardiac motions. Having demonstrated the feasibility of algorithm through the phantom data, the method was applied to phantom PET simulated data. Investigations of non-gated and gated images by comparing cross section views, activity profiles, contrast-to-noise ratios (CNRs) and left ventricle myocardium width of gated images showed an improvement compared with non-gated studies.

Methods

A. Phantom preparation

Average male torso produced by the non-uniform rational b-splines (NURBS)-based cardiac torso (NCAT) phantom (27) was used for simulations. The NCAT phantom is a four-dimensional (4D) digital phantom that is developed to provide a realistic and flexible model of the human anatomy and physiology. The organ shapes of this phantom are modeled based on non-uniform rational b-splines, NURBS, surfaces. These are continuous surfaces that allow the phantom to be produced at any spatial resolution. The NURBS surfaces can be easily altered so that the NCAT phantom can closely model variations in anatomy as well. 4D tagged magnetic resonance imaging (MRI) data as the basis for the cardiac model and 4D respiratory gated CT data as the basis for the respiratory model were used to extend the phantom to model the cardiac and respiratory motions (27). Both the activity phantom containing the radioactive distribution and attenuation phantom containing tissue attenuation distribution at any spatial resolution can be generated using the NCAT.

In this study the diaphragmatic motion was 2 cm, based on diaphragmatic motion during normal respiration (5) and the respiratory cycle was 5 s containing 5 cardiac cycles. The respiratory cycle was divided equally into 80 phases, 0.0625 s each, for analysis purposes. Two 128×128×128 three-

dimensional phantoms, one as activity and the other as attenuation distribution were generated by the NCAT for every 80 phases in the respiratory cycle. Phases 1 and 40 corresponded to end of exhalation and end of inhalation respectively. The 80 respiratory gated images were produced with the heart at 16 different point of the cardiac cycle. The activity phantoms contained a homogeneous distribution of activity in the myocardium as a healthy heart. The activity distributions in phantom, similar to work by Fitzpatrick et al, were set based on FDG uptake on normal human experiments (3, 28-29) and the attenuation phantoms were generated based on zubal coefficients (30).

B. PET simulation

Emission sinograms were generated using Eidolon (31), an object-oriented Monte Carlo simulation software package for 3D PET acquisition modeling (31, 32). The scanner parameters were configured to simulate the B-HIRZ scanner (Somatom Sensation 16; Siemens Medical Solutions), a LSO-based high resolution whole-body PET scanner. This scanner has no septa, thus only 3D acquisitions are allowed. The detector ring is made of 144 blocks containing 169 crystals that were 4×4×20 mm^3 and arranged in a 13×13 array. This includes a 162 mm axial field of view with 39 rings generating 81 image planes. The acceptance energy window is set to 425-650 keV. The scanner that includes LSO crystal detector planes, has a very short coincidence time resolution about 500 ps and a 15% overall system energy resolution. A total of 24336 crystals build the rings with a diameter of 83 cm. The number of decays specified for each simulation was 1600 million, which resulted in approximately 105 million true coincidences; in agree with American society of nuclear cardiology practice guidelines (33).

C. Reconstruction and data analysis

All sinograms reconstructed using an iterative reconstruction algorithm based on ordered-subset expectation maximization (OSEM) that has been shown to improve the resolution, image contrast, and signal-to-noise ratio compared with FBP with at least equal quantitative accuracy in some clinical studies (34-37). Arc correction was applied on emission data sets. No scatter and attenuation correction techniques were applied. To evaluate the effects at all cardiac phases, each of the 16 different cardiac phases were processed separately.

To represent respiratory motion corrected data with respect to the cardiac cycle, the algorithm applied to five emission data with the heart at same point of cardiac cycle. The algorithm summed emission data sets after finding the adequate values of x, y and z (z direction represented body long axis) shifts of each one to produce the best *RMC* cardiac PET images. This process was repeated for all of 16 cardiac phases. To produce PET data sets with no respiratory motion correction, the activity data sets were registered with no manipulations, so we considered this case by summing the five emission data sets with the heart at same point of cardiac cycle without using the found adequate shifts. This process was also repeated for all of 16 cardiac phases. Finally, both processes were repeated for all simulations. To evaluate the effect of respiratory motion correction on CNRs, two freehand regions of interest (RIOs) were drawn over left ventricle myocardium region of PET images. To estimate the noise, background freehand ROIs were drawn on the left ventricle cavity of PET images. To minimize the influence of the operator dependent errors in the ROI drawing and positioning, ROIs were drawn over respiratory motion corrected (*RMC*) images and then we loaded same ROIs over the non-*RMC* images. Signal and noise values were automatically obtained and the operator needed only to get data sets related to all ROIs. The left ventricle myocardium contrast recovery coefficient (Q_m) was calculated as follow:

$$Q_m = \frac{(Cmyo_{RMC} / Cbkg_{RMC})}{(Cmyo_{nc} / Cbkg_{nc})}, \quad (1)$$

where $Cmyo$ is the average of counts measured in the ROIs drawn over the left ventricle region of the images and $Cbkg$ is the average of counts measured in the ROIs drawn over the left ventricle cavity of the images. Index of *RMC* refers to *RMC* PET images and index of *nc* refers to non-*RMC* PET images. To evaluate the activity profiles and left ventricle myocardium width, two perpendicular line profiles were drawn over the *RMC* and non-*RMC* images. To minimize the influence of the operator in the line profiles drawing and positioning, the first line profile was saved and loaded over all other images and the operator needed only to get data sets related to all images.

Results

The simplest, although somewhat subjective, measure of image quality is visual appearance (4). Figure 1(a) shows the non-*RMC* image of heart region. This image is blurred, and smearing effects were quite evident visually, making the anteroapical region and

lateral wall of the left ventricle appear with approximately 1.38 and 1.12 times the values obtained for *RMC* image that is shown in Fig. 1(b), respectively.

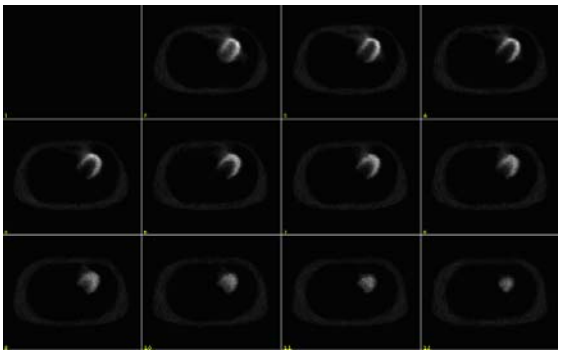

(a)

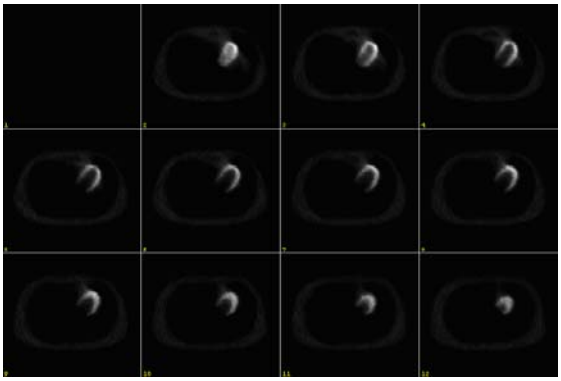

(b)

Fig 1. Respiratory motion correction applied to PET cardiac images. Left ventricle myocardium images (a) before respiratory motion correction and (b) after respiratory motion correction. Two perpendicular line profiles are shown by a vertical and a horizontal line.

Even though the myocardium widths of non-*RMC* images were greater than the values related to *RMC* images, the respiratory motion correction was successful and provided a significantly realized image. In this study, the non-*RMC* and *RMC* images were visualized in the transverse planes, showing the differences between quantified values. Comparing the Q_m values shows that the applied correction affected phases of number 7,8 and 9 of cardiac cycle more than the other phases. The maximum value of Q_m was 1.43±0.07 for phase number 8 while it was 1.37±0.07 and 1.41±0.07 for phases of number 7 and 9 respectively. Figure 2 shows the Q_m calculated for different phases of cardiac cycles.

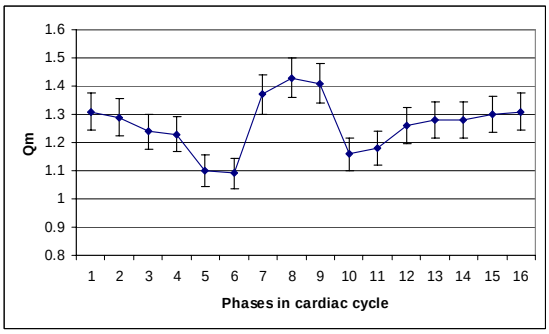

Fig 2. The left ventricle myocardium contrast recovery coefficients (Q_m).

All of the values calculated for Q_m were greater than one, and this shows that the applied correction, improved the CNR. To better evaluate the effect of applied respiratory motion correction, count of pixels along two perpendicular line profiles, cutting left ventricle myocardium, were evaluated. The location of first line was chosen such that the maximum $Cmyo/Cbkg$ along the apicobasal direction was the greatest. Location of the other line was perpendicular to the first line, passing the middle of lateral wall of the heart. Myocardium widths were determined over these two line profiles. The maximum value of ratio of the left ventricle myocardium width for non-*RMC* and *RMC* images along the line profile passing the apicobasal direction was 1.38±0.07 for phase number 9 and its value was 1.32±0.07 and 1.38±0.07 for phases of number 7 and 8 respectively. All of the values calculated for ratio of the left ventricle myocardium width for non-*RMC* and *RMC* images along the line profile passing the apicobasal direction were greater than one, and this shows that the applied correction, improved the CNR, too. Figure 3(a) shows the ratio of the left ventricle myocardium width for non-*RMC* and *RMC* images along the line profile passing the apicobasal direction. Similar ratio for line profile perpendicular to the first one, passing from the middle of the lateral wall of the left ventricle was calculated and the maximum value of ratio of the left ventricle myocardium width for non-*RMC* and *RMC* images along the line profile passing from the middle of the lateral wall of the left ventricle was 1.12±0.03 for phases of number 8 and

9. The similar value was 1.1±0.04 for phase number 7.

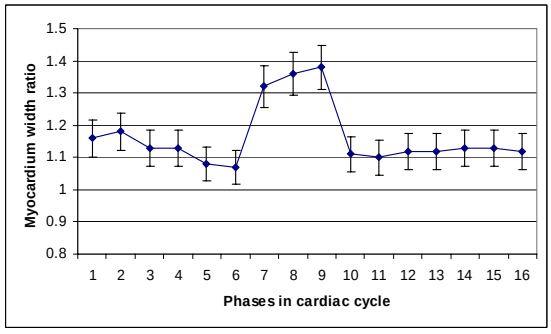

(a)

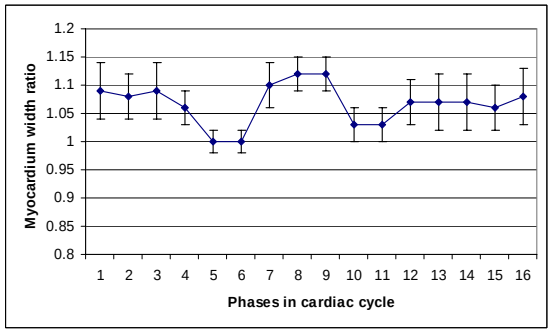

(b)

Fig 3. (a) Ratio of the left ventricle myocardium width for non-*RMC* and *RMC* images along the line profile passing the apexobasal direction. (b) Ratio of the left ventricle myocardium width for non-*RMC* and *RMC* images along the line profile passing the middle of heart lateral wall.

The minimum of the values calculated for ratio of the left ventricle myocardium width for non-*RMC* and *RMC* images along the line profile passing from the middle of the lateral wall of the left ventricle was one, and this shows that the applied correction, improved the CNR, as well. The ratio of the left ventricle myocardium width for non-*RMC* and *RMC* images along the line profile passing from the lateral wall of the left ventricle is shown in figure 3(b). Ratio of count profiles of *RMC* images and non-*RMC* images was calculated in different phases of the cardiac cycle. This demonstrated that the motion artifacts were reduced by respiratory motion correction and this effect, corrected spreading the radiotracer activity over an increased volume of myocardium, shown in Fig. 4(a) and 4(b). These images were formed by dividing the FWHM of count profiles of non-*RMC* images and *RMC* images for both perpendicular line profiles drawn over images.

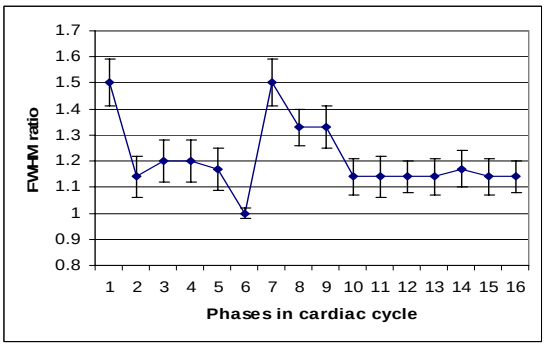

(a)

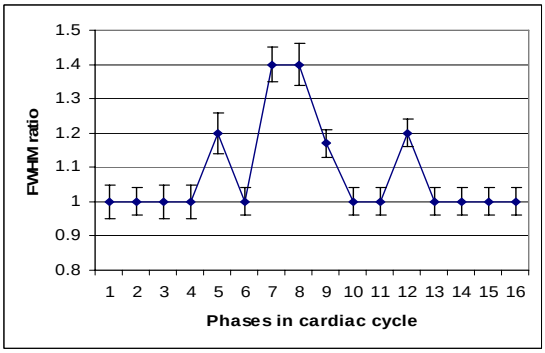

(b)

Fig 4. (a) Ratio of the count profile's FWHM for non-*RMC* and *RMC* images along the line profile passing the apexobasal direction. (b) Ratio of the count profile's FWHM for non-*RMC* and *RMC* images along the line profile passing the middle of heart lateral wall.

Discussion

In conducting cardiac PET simulations to examine the effects of respiratory motion on image quality, noticeable motion artifacts were found. Consistent with the findings of Fitzpatrick and Wells (3), Chin et al (38) and Thorndyke et al (4), we found that the amplitude and phase of diaphragmatic motion due to breathing have an important role in variations of respiratory-induced errors. These errors may result in blurring and ghosting artifacts reducing image quality that can be explained by the shift in organ position with respiration. Shift in heart position overestimates the myocardium width and underestimates the

myocardium activity distribution due to spreading the radiotracer activity over an increased volume. As an example, at the end of inhalation phase of respiratory cycle, the position of the heart is at its most superior position, resulting in lung tissue occupying the space that the heart was located at other points in that cycle and as mentioned before, this may reduces the image quality. To obtain accurate quantifiable cardiac images, respiratory motion should be compensated for or reduced by gating techniques (3, 6, 17).

Consistent with the findings of Fitzpatrick and Wells the variation in magnitude of the errors in the cardiac uptake varied considerably less with cardiac cycle than with respiratory cycle (3). This suggests that organ motion due to breathing produces a more significant artifact on cardiac PET images compared to the motion due to cardiac cycle. The simulation results demonstrated that respiratory motion correction could preserve myocardium shape, size and activity, which is important for accurate quantification in order to assess if the myocardial perfusion is irregular or changing. Improvement in accurate quantifiable cardiac imaging according to same cardiac phases due to respiratory motion correction is more pronounced in anteroapical region (Fig. 3(a)) as compared with the lateral wall (Fig. 3(b)). Investigation of these improvements showed variations at different cardiac phases. The maximum improvement of myocardium width for anteroapical region was about 38% for phase 9 of cardiac cycle while these values were 32% and 36%, for phases 7 and 8 respectively which are very close to the maximum value. Investigation of the effect of the applied correction on the heart lateral wall, showed a 12% improvement for phases 8 and 9. Similar calculations for other phases of cardiac cycle showed values between 1.00-1.10, which are all very close to maximum value. Similarly, CNR varied at different cardiac phases corresponding to the cycle and points. After the respiratory motion correction, the cardiac phases 7, 8 and 9 revealed a higher CNR than the other phases resulting to highest value of Q_m. The maximum variation of Q_m was about 43% obtained for phase 8 of cardiac cycle. Calculation of Q_m for phases 7 and 9 of cardiac cycle resulted in 37% and 41% improvement respectively which are very close to the maximum value. We expected some small variations in calculated ratios resulting from motion correction, but this study showed that diaphragmatic motion during respiratory phases may produce variations bigger than previously expected. Some researchers reported patient's abdomen monitoring as a way to determine the breathing motion of the chest wall (20, 39) as a useful way for respiratory gating. Thus to determine the role of diaphragmatic motion during different respiratory phases, we monitored the motion of phantom's abdomen and diaphragm during breathing. Figure 5 shows the result of phantom's abdomen monitoring during a normal breathing with a 2 cm diaphragmatic motion (5).

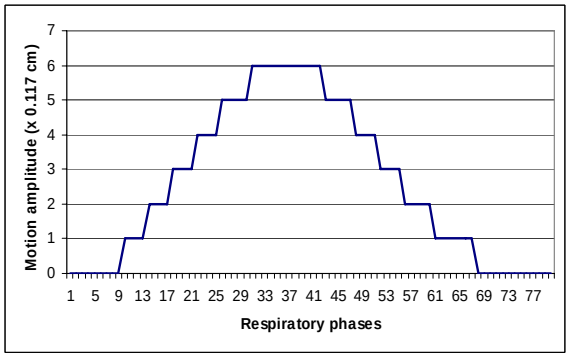

Fig 5. Amplitude of phantom's abdomen motion during a normal breathing with 2 cm diaphragmatic motion for different respiratory phases.

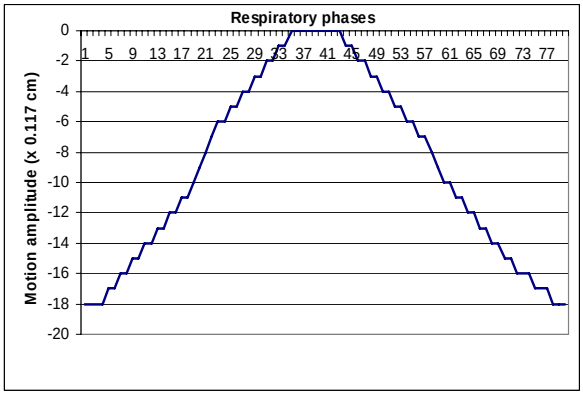

Fig 6. Amplitude of phantom's diaphragm motion during a normal breathing with 2 cm diaphragmatic motion for different respiratory phases.

Although the respiratory cycle is divided into 80 small parts, but diaphragmatic motion due to breathing, had the effect of spreading the signal in proportion to the time and phase of respiratory cycle. On the other hand, blurring and ghosting of each image depends on the speed of diaphragm during that respiratory phase. To determine the role of

diaphragmatic velocity on image quality, two indexes were related to each respiratory phase. These indexes were calculated as $\frac{1}{n}$ that n is the number of respiratory phases with diaphragm as first index and abdomen surface as the second index in the same slice. The position of diaphragm was determined by monitoring a 512×512×512 4D-NCAT phantom with cubic voxels of 0.117 cm as shown in Figure 6. The more calculated index showed that the diaphragm velocity was higher while passing that respiratory phase and more blurring and ghosting was expected in such image. Correction of respiratory motion using gating technique for all of 16 cardiac phases to represent *RMC* data with respect to the cardiac cycle was done using the correction algorithm and summing five emission data with the heart at the same point of cardiac cycle after corrections. To evaluate the entire effect of emission data sets of 5 respiratory phases summed to produce one cardiac phase, table 1 showed the sum of five related indexes.

Table 1. Indexes comparing the diaphragm velocity related to each cardiac phase. Index 1 and Index 2 calculated monitoring of abdomen surface motion and diaphragm motion respectively.

Cardiac phases	Index 1	Index 2
1	0.8373	2.2500
2	0.8373	2.2500
3	0.8373	2.3611
4	0.7713	2.3611
5	0.7713	2.6111
6	0.7713	2.6111
7	0.7713	2.1111
8	0.7213	1.9444
9	0.7213	1.9444
10	0.8102	2.4444
11	0.9269	2.4444
12	0.9269	2.3333
13	0.8697	2.3333
14	0.8697	2.3333
15	0.7531	2.3333
16	0.8031	2.3333

Both index series showed that diaphragm velocity has its own lower effect on cardiac phases 8 and 9. Comparing the CNR, Q_m and improvement of myocardium width ratios between different cardiac cycles shows an agreement with this finding. Index 2 series is highly more sensitive to diaphragm motion than index 1 series and it can be easily found comparing Fig. 5 and Fig. 6. Although it is shown here in this study that monitoring of diaphragm motion is more useful, but this monitoring can not be done easily in a clinical setting. To compensate for this, using an automatic algorithm capable of correcting respiratory motion using full signal may be very useful to prevent lengthening overall scan time to obtain same motionless lesion signal levels (4) because increasing in the scan time may causes some difficulties related to patient discomfort and immobilization (4, 24).

One limitation of our study was that scatter correction was not included in this study. Although scattered photons may influence the calculated quantities, we did not correct it to prevent any change in emission data sets because of in the presence of accurate scatter correction, it is expected that the noise in the projection data would increase, but the mean values and as a result the ratios would not changed and thus, including scatter and scatter correction in the simulations would not greatly change the general conclusions of this study (3).

Some additional limitations are related to body phantom's shape, size, breathing and cardiac cycles and diaphragmatic motion. In future studies using of different sizes of male and female phantoms can determine how the correction improves the image quality from one patient to another. Phantom's breathing and cardiac cycles, here in this study are perfectly normal and regular, whereas variations in respiratory and cardiac cycles from patient to patient and to time may also influence the observed effects in this study and may need to be incorporated in future studies. Amplitude of diaphragmatic motion and respiratory cycle during inhalation has a very important role in summing the phases together and may also differ from one patient to another. For example, if the amplitude of diaphragmatic motion in one patient is more than 2 cm (which differs from our simulated breathing pattern) the values in Fig.5 and Fig. 6, as well as the indexes of table 1 and thus cardiac phase of maximum CNR, Q_m and improvement of myocardium width ratios would vary. This would be due to a re-indexing of different respiratory phases.

One potential issue with using automatic algorithm to respiratory motion correction of PET data is that each of data sets (in our simulation 80) can be compared with other phases in similar point of cardiac phase, with no need to perform abdominal monitoring.

Acknowlegment

We would like to thank W. Segars, F. Schoenahl and M.R. Ay for their support and guidance on this project.

References

1. Di Carli MF, Hachamovitch R. Should PET replace SPECT for evaluating CAD? The end of the beginning. J Nucl Cardiol. 2006; 13: 2-7.
2. Fitzpatrick MJ, starkschall G, Balter P, Antolak JA, Guerrero T, Nelson C, Keall P and Mohan R. A novel platform simulating irregular motion to enhance assessment of respiration-correlated radiation therapy procedures. J Appl Clin. 2005; 6: 13-21.
3. Fitzpatrick GM, Wells GR. Simulation study of respiratory-induced errors in cardiac positron emission tomography/computed tomography. Med Phys. 2006; 33: 2888-2895.
4. Thorndyke B, Schreibmann E, Koong A, Xing L, Reducing respiratory motion artifacts in positron emission tomography through retrospective stacking. Med Phys. 2006; 33: 2632-2641.
5. Desjardins T. Cardiopulmonary Anatomy and Physiology, 4th Ed. New York, Delmar Thomson Learning Inc. 2002.
6. Boucher L, Rodrigue S, Lecomte R, Benard F. Respiratory gating for 3-dimensional PET of the thorax: Feasibility and initial results. J Nucl Med. 2004; 45: 214- 219.
7. Pitman AG, Klaff V, Van Every B, Risa B, Barnden LR, Kelly MJ. Effect of mechanically simulated diaphragmatic respiratory motion on myocardial SPECT processed with and without attenuation correction. J Nucl Med. 2002; 43: 1259-1267.
8. Caldwell CB, Mah K, Skinner M. Can PET provide the 3D extent of tumor motion for individualized internal target volumes? A phantom study of the limitations of CT and the promise of PET. Int J Radiat Oncol Biol Phys. 2003; 55: 1381-1393.
9. Sarikaya I, Yeung HW, Erdi Y, Larson SM. Respiratory artifact causing malpositioning of liver dome lesion in right lower lung. Clin Nucl Med. 2003; 28: 943- 944.
10. Suga K, Kawakami Y, Zaki Z, Yamashita T, Shimizu K, Matsunaga N. Clinical utility of co-registered respiratory-gated ^{99m}Tc-Technegas/MAA SPECT-CT images in the assessment of regional lung functional impairment in patients with lung cancer. Eur J Nucl Med Mol Imaging. 2004; 31: 1280-1290.
11. Boucher L, Rodrigue S, Lecomte R, Benard F. Respiratory gating for 3-dimensional PET of the thorax: Feasibility and initial results. J Nucl Med. 2004; 45: 214- 219.
12. Nehmeh SA, Erdi YE, Rosenzweig KE, Humm JL, Yorke ED, Squire OD, Ford E, Sidhu K, Mageras G, Braban LE, Larson SM, Ling CC. Effect of respiratory gating on reducing lung motion artifacts in PET imaging of lung cancer. Med Phys. 2002; 29: 336-371.
13. Ritchie CJ, Crawford CR, Godwin JD, King KF, Kim Y. Correction of computed tomography motion artifacts using pixel-specific back-projection. IEEE Trans Med Imaging. 1996; 15**:** 333–42.
14. Cho K, Kumiata SI, Okada S, Kumazaki T. Development of respiratory gated myocardial SPECT system. J Nucl Cardiol. 1999; 6: 20-28.
15. Tsui BMW, Segars WP, Lalush DS. Effects of upward creep and respiratory motion in myocardial SPECT. IEEE Trans Nucl Sci. 2000; 47: 1192-1195.
16. Berne RM, Levy MN. Physiology St.Louis, MO: Mosby year book, 1998.
17. Huesman R, Klein G, Reutter B. Respiratory compensation in cardiac PET using doubly-gated acquisitions. J Nucl Med. 1997; 38: 114P.
18. Klein GJ, Reutter, Ho MH, Reed JH, Huesman RH. Real-time system for respiratory-cardiac gating in positron tomography. IEEE Trans Nucl Sci. 1998; 45: 2139-2143.
19. Nehmeh SA, Erdi YE, Ling CC, Rosenzweig KE, Schoder H, Larson SM, Macapinlac HA, Squire OD, Humm JL. Effect of respiratory gating on quantifying PET images of lung cancer. J Nucl Med. 2002; 43: 876-881.

20. Nehmeh SA, Erdi YE, Rosenzweig KE, Schoder H, Larson SM, Squire OD, Humm JL. Reduction of respiratory motion artifacts in PET imaging of lung cancer by respiratory correlated dynamic PET: methodology and comparison with respiratory gated PET. J Nucl Med. 2003; 44: 1644-1648.
21. Boucher L, Rodrigue S, Lecomte R, Benard F. Respiratory gating for 3-dimensional PET of the thorax: Feasibility and initial results. J Nucl Med. 2004; 45: 214- 219.
22. Livieratos L, Rajappan K, Stegger L, Schafers K, Bailey DL, Camici PG. Respiratory gating of cardiac PET data in list-mode acquisition. Eur J Nucl Med Mol Imaging. 2006; 33: 584-588.
23. Li T, Thorndyke B, Schreibmann E, Yang Y, Xing L. Model-based image reconstruction for four-dimensional PET. Med Phys. 2006; 33: 1288-1298.
24. De Juan R, Seifert B, Berthold T, von Schulthess GK, Goerres GW. Clinical evaluation of a breathing protocol for PET/CT. Eur Radiol. 2004; 14: 1118-1123.
25. Klein GJ, Reutter BW, Huseman RH. Non-rigid summing of gated PET via optical flow. IEEE Trans Nucl Sci. 1997; 44: 1509-1512.
26. Livieratos L, Stegger L, Bloomfield PM, Schafers K, Bailey DL, Camici PG. Rigid-body transformation of list-mode projection data for respiratory motion correction in cardiac PET. Phys Med Biol. 2005; 50: 3313-3322.
27. Segars W, Tsui B. Study of the efficacy of respiratory gating in myocardial SPECT using the new 4D NCAT phantom. IEEE Trans Nucl Sci. 2002; 49: 675-679.
28. Matsunari I, Kanayama S, Yoneyama T, Matsudaira M, Nakajima K, Taki J, Nekolla SG, Takekoshi N, Tonami N, Hisada K. Myocardial distribution of 18F-FDG and 99mTc-sestamibi on dual-isotope simultaneous acquisition SPET compared with PET. Eur J Nucl Med. 2002; 29**:** 1357–1364.
29. Hays M, Watson E, Thomas S, Stabin M. MIRD dose estimate report No. 19: Radiation absorbed dose estimate from ^{18}F-FDG. J Nucl Med. 2002; 43: 210-214.
30. Zubal IG, Harrell CR, Smith EO, Rattner Z, Gindi G, Hoffer PB. Computerized three-dimensional segmented human anatomy. Med Phys. 1994; 21: 299–302.
31. Zaidi H, Scheurer AH, Morel C. An object-oriented Monte Carlo simulator for 3D positron tomography. Comput Methods Programs Biomed. 1999; 58:133-145.
32. Buvat I, Castiglioni I. Monte Carlo simulation in SPET and PET. Q J Nucl Med. 2002; 46: 48-61.
33. Bacharach SL, Bax JJ, Case J, Delbeke D, Kurdziel KA, Martin WH, Patterson RE. American society of nuclear cardiology practice guidelines. 2003; 10: 543-554.
34. Boellaard R, van Lingen A, Lammertsma AA. Experimental and clinical evaluation of iterative reconstruction (OSEM) in dynamic PET: quantitative characteristics and effects on kinetic modeling. J Nucl Med. 2001; 42: 808–817.
35. Koepfli P, Hany TF, Wyes CA, Namdar M, Burger C, Konstantinidis AV, Berthold T, VonSchulthess GK, Kaufmann PA. CT Attenuation Correction for Myocardial Perfusion Quantification Using a PET/CT Hybrid Scanner. J Nucl Med. 2004; 45: 537–542.
36. Van der Weerdt AP, Boellaard R, Knaapen P, Visser CA, Lammertsma AA, Visser FC. Postinjection transmission scanning in myocardial 18F-FDG PET studies using both filtered backprojection and iterative reconstruction. J Nucl Med. 2004; 45: 169-175.
37. Brambilla M, Secco C, Dominietto M, Matheoud R, Sacchetti G, Inglese E. Performance characteristics obtained for a new 3-dimensional lutetium oxyorthosilicate-based whole-body PET/CT scanner with the National electrical manufacturers association NU 2-2001 standard. J Nucl Med. 2005; 46: 2083-2091.
38. Chin B, Nakamoto Y, Kraitchman D, Marshall L, Wahl R. PET-CT evaluation of 2-deoxy-2-[18F]fluoro-D-glucose myocardial uptake: effects of respiratory motion. Mol Imag Bio. 2001; 5: 57-64.
39. Dawood M, Lang N, Jiang X, Schafers KP. Lung motion correction on respiratory gated 3D. PET/CT images. IEEE Trans Med Imaging. 2006; 25(4): 476-485.